Experimental bifurcation-cascade diagram of an external-cavity semiconductor laser

Byungchil Kim, Nianqiang Li, A. Locquet, D. S Citrin

Experimental bifurcation-cascade diagram of an external-cavity semiconductor laser

Byungchil Kim,[1,2,*] **Nianqiang Li,**[3,1] **A. Locquet,**[2,1] **and D. S. Citrin**[1,2]

[1]*Georgia Institute of Technology, School of Electrical and Computer Engineering, Atlanta, Georgia 30332-0250 USA*

[2]*UMI 2958 Georgia Tech-CNRS, Georgia Tech Lorraine, 2 Rue Marconi F-57070, Metz, France*

[3]*Centers for Information Photonics and Communications, Southwest Jiaotong University, Chengdu, 610031 China*

[*]*gtg403z@mail.gatech.edu*

Abstract: This Letter is the first to report experimental bifurcation diagrams of an external-cavity semiconductor laser (ECSL) in the low-to-moderate current injection regime and long-cavity case. Based on the bifurcation cascade behavior which was unveiled by Hohl and Gavrielides [Phys. Rev. Lett. **82**, 1148-1151 (1999)], we present a detailed experimental investigation of the nonlinear dynamics of ECSLs and of the robustness of the cascade to changes in the current and cavity length. Also, we report for the first time a well resolved experimental Hopf bifurcation in an ECSL. Based on the Lang and Kobayashi model, we identify the dynamical regimes and the instabilities involved in the cascade, as well as the influence of the current and cavity length on the cascade.

OCIS codes: (140.1540) Chaos Lasers; (140.2020) Diode lasers; (140.5960) Semiconductor lasers; (190.3100) Instabilities and chaos.

References and links

1. C. Masoller and N. B. Abraham, "Stability and dynamical properties of the coexisting attractors of an external-cavity semiconductor laser," Phys. Rev. A **57,** 1313–1322 (1998).
2. J. Mork, J. Mark, and B. Tromborg, "Route to chaos and competition between relaxation oscillations for a semiconductor-laser with optical feedback," Phys. Rev. Lett. **65,** 1999–2002 (1990).
3. G. H. M. van Tartwijk and G. P. Agrawal, "Laser instabilities: a modern perspective," Prog. Quantum Electron. **22,** 43–122 (1998).
4. J. Ohtsubo, *Semiconductor Lasers-Stability, Instability and Chaos* (Springer, Berlin, 2006).
5. D. Brunner, X. Porte, M. C. Soriano, and I. Fischer, "Real-time frequency dynamics and high-resolution spectra of a semiconductor laser with delayed feedback," Sci. Rep. **2,** 732 (2012).
6. D. Rontani, M. Sciamanna, A. Locquet, and D. S. Citrin, "Multiplexed encryption using chaotic systems with multiple stochastic-delayed feedbacks," Phys. Rev. E **80**, 066209 (2009).
7. A. Argyris, D. Syvridis, L. Larger, V. Annovazzi-Lodi, P. Colet, I. Fischer, J. Garcia-Ojalvo, C. R. Mirasso, L. Pesquera, and K. A. Shore, "Chaos-based communications at high bit rates using commercial fiber-optic links," Nature **438,** 343–346 (2005).
8. W. L. Zhang, W. Pan, B. Luo, X. H. Zou, M. Y. Wang, and Z. Zhou,"Chaos synchronization communication using extremely unsymmetrical bidirectional injections," Opt. Lett. **33**, 237–239 (2008).
9. F. Y. Lin and J. M. Liu, "Chaotic lidar," IEEE J. Sel. Top. Quantum Electron. **10,** 991–997 (2004).
10. A. Uchida, K. Amano, M. Inoue, K. Hirano, S. Naito, H. Someya, I. Oowada, T. Kurashige, M. Shiki, S. Yoshimori, K. Yoshimura, and P. Davis, "Fast physical random bit generation with chaotic semiconductor lasers," Nat. Photon. **2,** 728–732 (2008).

#200290 - $15.00 USD Received 7 Nov 2013; revised 20 Jan 2014; accepted 20 Jan 2014; published 28 Jan 2014

11. M. C. Soriano, J. Garcia-Ojalvo, C. R. Mirasso, and I. Fischer, "Complex photonics: Dynamics and applications of delay-coupled semiconductors lasers," Rev. Mod. Phys. **85,** 421–470 (2013).
12. Y. Paquot, F. Duport, A. Smerieri, J. Dambre, B. Schrauwen, M. Haelterman, and S. Massar, "Optoelectronic Reservoir Computing," Sci. Rep. **2,** 287 (2012).
13. J. Mork, B. Tromborg, and J. Mark, "Chaos in semiconductor lasers with optical feedback: theory and experiment," IEEE J. Quantum Electron. **28,** 93–108 (1992).
14. J. Ye, H. Li, and J. McInerney, "Period-doubling route to chaos in a semiconductor laser with weak optical feedback," Phys. Rev. A **47,** 2249–2252 (1993).
15. T. Heil, I. Fischer, and W. Elsasser, "Coexistence of low-frequency fluctuations and stable emission on a single high-gain mode in semiconductor lasers with external optical feedback," Phys. Rev. A **58,** R2672–R2675 (1998).
16. S. Wieczorek and W. W. Chow,"Bifurcations and chaos in a semiconductor laser with coherent or noisy optical injection," Opt. Commun. **282,** 2367–2379 (2009).
17. K. Green, B. Krauskopf, F. Marten, and D. Lenstra,"Bifurcation Analysis of a Spatially Extended Laser with Optical Feedback," SIAM J. Appl. Dyn. Syst. **8,** 222–252 (2009).
18. I. V. Ermakov, G. Van der Sande, and J. Danckaert,"Semiconductor ring laser subject to delayed optical feedback: Bifurcations and stability," Commmun. Nonlinear Sci. and Numer. Simulat. **17,** 4767–4779 (2012).
19. R. J. Reategui, A. V. Kir'yanov, A. N. Pisarchik, Y. O. Barmenkov, and N. N. Il'ichev, "Experimental study and modeling of coexisting attractors and bifurcations in an erbium-doped fiber laser with diode-pump modulation," Laser Phys. **14,** 1277–1281 (2004).
20. S. Valling, B. Krauskopf, T. Fordell, and A. M. Lindberg, "Experimental bifurcation diagram of a solid state laser with optical injection," Opt. Commun. **271,** 532–542 (2007).
21. F. T. Arecchi, R. Meucci, G. Puccioni, and J. Tredicce, "Experimental evidence of subharmonic bifurcations, multistability, and turbulence in a Q-switched gas laser," Phys. Rev. Lett. **49,** 1217–1220 (1982).
22. A. P. A. Fischer, O. K. Andersen, M. Yousefi, S. Stolte, and D. Lenstra,"Experimental and theoretical study of filtered optical feedback in a semiconductor laser," IEEE J. Quantum Electron. **36,** 375–384 (2000).
23. R. Lang and K. Kobayashi, "External optical feedback effects on semiconductor injection-laser properties," IEEE J. Quantum Electron. **16,** 347–355 (1980).
24. A. Hohl and A. Gavrielides, "Bifurcation cascade in a semiconductor laser subject to optical feedback," Phys. Rev. Lett. **82,** 1148–1151 (1999).
25. A. Ritter and H. Haug,"Theory of laser-diodes with weak optical feedback .2. limit- cycle behavior, quasi-periodicity, frequency locking, and route to chaos," J. Opt. Soc. Am. B-Opt. Phys.**10,** 145–154 (1993).
26. C. H. Henry and R. F. Kazarinov, "Instability of semiconductor-lasers due to optical feedback from distant reflectors," IEEE J. Quantum Electron. **22,** 294–301 (1986).
27. T. Heil, I. Fischer, W. Elaassser, J. Mulet, and C. R. Mirasso,"Statistical properties of low-frequency fluctuations during single-mode operation in distributed-feedback lasers: experiments and modeling," Opt. Lett. **24,** 1275–1277 (1999).
28. F. R. Ruiz-Oliveras and A. N. Pisarchik, "Synchronization of semiconductor lasers with coexisting attractors," Phys. Rev. E **79,** 016202 (2009).

1. Introduction

The dynamics of external-cavity semiconductor lasers (ECSLs) are known to be complex and difficult to control; in view of the rich dynamical behavior as well as the technological importance of these devices, the dynamics have been widely investigated [1–5]. Nevertheless, experimental investigations have suffered from limitations that have made it difficult to obtain bifurcation diagrams (BDs) and access the frequency dynamics [5]. Until a few years ago, this chaotic behavior of semiconductor systems was viewed as an unwanted irritation to be engineered away. Nowadays, rather than simply being avoided, such dynamical instabilities are of intense interest for applications, such as secure communications [6–8], light detection and ranging(LIDAR) [9], random-number generation [4, 10, 11], and reservoir computing [12].

Various types of chaotic transitions of long-cavity ECSLs have been identified experimentally under specific conditions of cavity length L, injection current I, and feedback strength. A common transition is the quasi-periodic route to chaos [13], in which a stable external-cavity mode (ECM) is replaced by an attracting periodic orbit at a frequency close to the relaxation-oscillation frequency f_{RO} of the solitary laser, and this periodic attractor turns into a torus as the feedback strength increases. In addition, a period-doubling route to chaos has been reported [14]. In this case, a cascade of period-doubling bifurcations, creating oscillations at

#200290 - $15.00 USD Received 7 Nov 2013; revised 20 Jan 2014; accepted 20 Jan 2014; published 28 Jan 2014

frequencies close to sub-multiples of f_{RO}, occurs. Moreover, when the operating conditions are such that several ECMs are destabilized simultaneously, generalized multistability occurs as several attractors or attractor ruins coexist in phase space [1] and numerous phenomena related to attractor switching can be expected to be observed in a bifurcation diagram; an example is the switching between a low-frequency-fluctuation (LFF) state and a state of stable emission reported in [15].

Important insight into the dynamics of a system can often be gained by determining a BD obtained by fixing all but one parameter and then mapping out the extremal values of a dynamical variable as that parameter is varied. It provides an easily apprehended depiction of how the dynamics undergo transitions between qualitatively different regimes as the control variable is changed. Several theoretical and numerical works have studied in detail the bifurcation diagrams of ECSLs as a function of the feedback strength such as a single-mode semiconductor laser [16], vertical cavity surface-emitting lasers [17], and ring lasers [18]. Also, some experimental BDs for Er-doped fiber lasers [19], optically injected solid-state lasers [20], and gas lasers [21] have been mapped out. However, there is an almost total lack of experimental BDs available for ECSLs because there are several experimental hurdles that need not necessarily be resolved for more restricted studies. Especially for ECSLs, BDs require a precise control of the amount of feedback and accurate, stable, thermal and mechanical controls, which are difficult to achieve [22]. Even though there are numerous studies of the dynamics of ECSLs in restricted regimes, yet a comprehensive picture—and on that reconciled experiment and theory across a range of operating parameters—remained, surprisingly, until now unavailable. There is a need for such measurements as they provide a way to test the reliability of models for the laser dynamics, such as the Lang and Kobayashi (LK) model [23].

Our Letter reports experimental BDs of an ECSL that the closest operation conditions were in [24], where Hohl and Gavrielides focused on the case of an ECSL biased just above threshold and subjected to feedback from a distant reflector (long-cavity case) and observed a cascade of bifurcations between ECMs. Importantly, we reiterate: the results map out, for the first time to our knowledge, detailed bifurcation diagrams of ECSLs as function of a feedback strength for various L and I, thus covering a significant portion of parameter space. We have grounded our discussion in the extensive theoretical studies based on the LK equations and observed a cascade of BDs in accordance with our experimental results.

2. Experimental setup

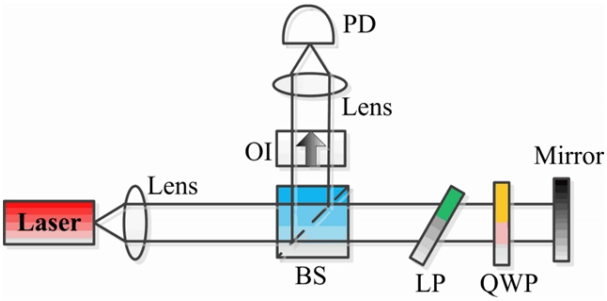

Fig. 1. Experimental setup. PD: photodiode, BS: beam splitter, LP: linear polarizer, Q: quarter-wave plate, M: mirror, OI: optical isolator.

The experimental setup is shown in Fig. 1. Light from the laser-diode is split into two free-space optical paths using a beam splitter (BS). One optical path is used for feedback into the

#200290 - $15.00 USD Received 7 Nov 2013; revised 20 Jan 2014; accepted 20 Jan 2014; published 28 Jan 2014

laser-diode and the other is for coupling and/or observing the dynamics of the intensity detected at the photodiode. The semiconductor laser used in our experiments is an intrinsically single-longitudinal mode InGaAsP DFB laser that oscillates at wavelength 1550 nm with maximum power of 15 mW. The free-running threshold current (I_{th}) is 9.27 mA. A real-time oscilloscope with 12 GHz bandwidth is used to capture the time series of the optical intensity. We also measure the RF spectrum with a spectrum analyzer with 23 GHz bandwidth and the optical spectrum with a scanning Fabry-Perot interferometer of 10 GHz free spectral range and finesse equal to 150. L is chosen to be 15, 30, or 65 cm corresponding to external-cavity round time τ = 1, 2, or 4.3 ns, respectively.

In order to overcome the experimental challenges encountered in such a broad study, it is necessary to have highly stabilized temperature (temperature stability / 24 hours $< 0.002\ ^{\circ}$ C) and I (drift / 24 hours $< 100\ \mu$A). Also, the experimental feedback strength η is controlled by minutely and slowly changing, with a motorized rotation stage, the angle of the quarter-wave plate (QWP) in the external cavity. This allows for very good horizontal resolution of the BDs; indeed, the rotation velocity is 0.01 degree/minute and the resolution of the angle of QWP is 1/100 degree, leading to a 4500 possible different values of the feedback in a BD. Maximum feedback, corresponding to η=1.0, is reached when the QWP angle is such that the polarization is not subjected to any rotation. In that case, $\sim$20% of the optical power is fed back onto the collimating lens.

3. Biufurcation-cascade diagram

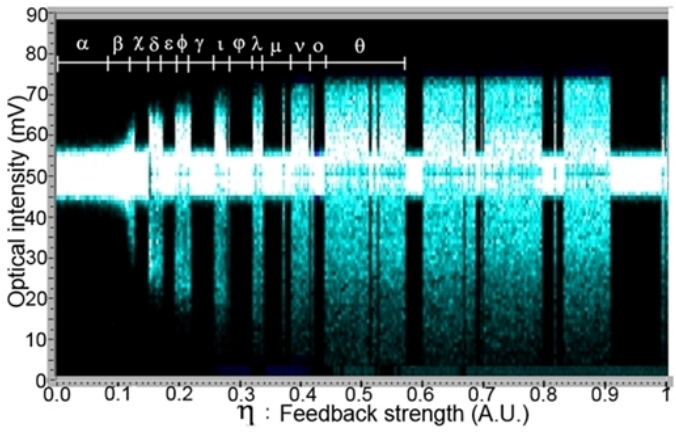

Fig. 2. Experimental BD of I=11.24 mA and L=30 cm.

Figure 2 shows the experimentally observed BD for I = 11.24 mA. Here L = 30 cm, resulting in a frequency spacing between ECMs of $\sim$500 MHz. The experimental BD is obtained by taking the local extrema of the intensity time series from the high-speed oscilloscope used in the experiment as a function of η. Density is high in white (blue in the color figure) but low in black regions. A bifurcation cascade between apparently stable and unstable regions is observed. Because of the low current chosen, the photodetected optical intensity is weak and does not always stand out of system noise. Consequently, the thinner regions in the optical intensity, that we call stable, do not necessarily correspond to stable CW behavior but also contain regimes in which instabilities around a single ECM have developed. The wider regions in the optical intensity, referred to as unstable regions, typically correspond to regimes in which trajectories wander around several ECMs and thus clearly stand out of noise.

#200290 - $15.00 USD Received 7 Nov 2013; revised 20 Jan 2014; accepted 20 Jan 2014; published 28 Jan 2014

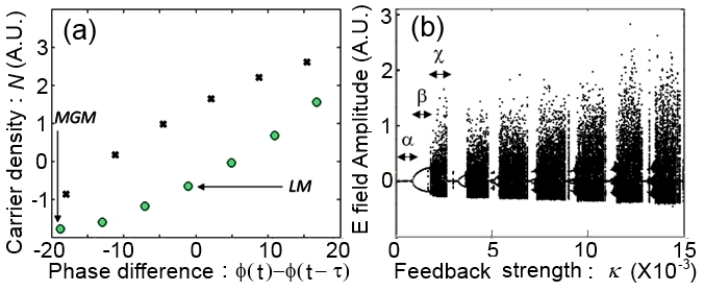

Fig. 3. (a) Ellipse structure of fixed points in the phase-difference-vs.-N plane for $\kappa = 0.009$ and $\tau = 1$ ns. (b) Numerical BD of $p = 1.03$ and $L = 15$ cm ($\tau = 1$ ns).

The single-longitudinal-mode description of a semiconductor laser in terms of rate equations has proven to be a fruitful approach for analyzing the dynamics. Clearly, the LK equations integrate out spatial degrees of freedom, therefore obviation the possibility of accounting in a detailed fashion for a number of effects. Nonetheless, while obtaining perfect correspondence between theory and experiment for identical parameters is not to be expected, the LK equations have reliably predicted trends in the dynamical behavior as a function of various parameters [25], and is widely employed. The LK model in the external cavity is described by three parameters: theoretical feedback strength κ, proportional to η, delay time τ, proportional to L, and the feedback phase $\omega_o\tau$, which is the product of τ and the solitary laser angular frequency ω_o.

The LK equations for the complex amplitude $E(t)$ and the carrier density $N(t)$ are

$$\frac{dE}{dt} = \frac{1+i\alpha}{2}\left(\mathscr{G} - \frac{1}{\tau_p}\right)E(t) + \frac{\kappa}{\tau_{\text{in}}}E(t-\tau)e^{-i\omega_o\tau}, \tag{1}$$

$$\frac{dN}{dt} = pJ_{\text{th}} - \frac{N(t)}{\tau_s} - \mathscr{G}|E|^2. \tag{2}$$

Here, $\mathscr{G} = G[N(t) - N_o]$ is the optical gain where G is the gain coefficient and N_o is the carrier density at transparency. Other parameters are τ_p, photon lifetime; τ_s, carrier lifetime; τ_{in}, optical round-trip time within the laser cavity; α, linewidth enhancement factor; p, pumping factor ; J_{th}, threshold current. We numerically integrated Eqs. (1) and (2) with the following parameters: $G = 8.1 \times 10^{-13}$ m^{3}s^{-1}, $N_o = 1.1 \times 10^{24}$ m^{-3}, $\tau_p = 1$ ps, $\tau_s = 1$ ns, $\tau_{\text{in}} = 8$ ps, $\alpha = 3$, and $\omega_o\tau = 0$.

Two kinds of CW solutions of Eqs. (1) and (2) exist: the ECMs that can be stable and the antimodes that are unstable saddle points [1]. These CW solutions are plotted in the plane of carrier density $N(t)$ versus phase difference $\Delta\phi(t) = \phi(t) - \phi(t-\tau)$ in Fig. 3(a). In this plane, ECMs and antimodes are known to lie on an ellipse [26]. ECMs are marked with circles and antimodes are marked with crosses. Among ECMs, two stand out: the minimum linewidth mode (LM) and the maximum gain mode (MGM). The MGM is the one with the lowest frequency (high gain end of the ellipse), and is usually stable [1, 15]. The LM is the closest ECM in frequency to the solitary laser mode.

The simulated BD of the AC part of the optical intensity as a function of κ is shown in Fig. 3(b). To mimic the experimental conditions in which η is gradually increased, the initial state, for a given κ, is selected to be equal to the final state of the simulation corresponding to the previous, smaller, value of κ. It is clear that, like in the experiment, alternating stable and unstable regions are observed. We show, in Fig. 4, the trajectory in (N, $\Delta\phi$) plane. The scenario of

#200290 - $15.00 USD Received 7 Nov 2013; revised 20 Jan 2014; accepted 20 Jan 2014; published 28 Jan 2014

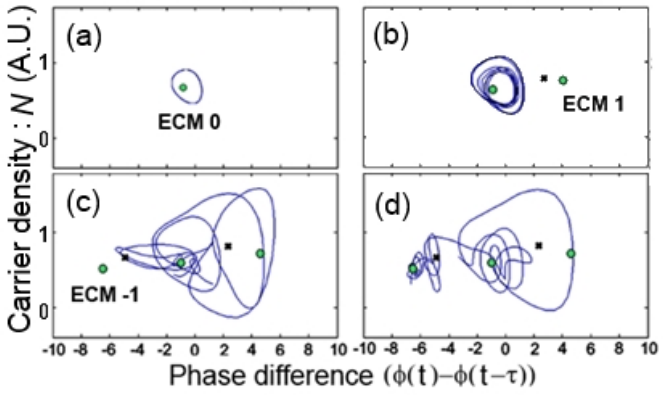

Fig. 4. Trajectory in phase space at τ = 1 ns. The circle indicates an ECM and the cross indicates an antimode (a) κ = 0.0014(limit cycle), (b) 0.002(quasi-period), (c) 0.0036, and (d) 0.00375.

the onset of the cascade bifurcation is as described in Ref. [24]; without feedback, there is only one fixed point that corresponds to the emission mode of the solitary laser. As κ increases from 0 to 0.0014 [Fig. 3(b)α], the first ECM 0, is initially stable and is then destabilized by bifurcations, starting with a Hopf bifurcation [Figs. 3(b)β and 4(a)]. Two pairs of new fixed points are sequentially created by increasing κ: ECM 1 and the corresponding antimode [Fig. 4(b)], followed by ECM -1 (the MGM) and the corresponding antimode [Fig. 4(c)]. The trajectory wanders around ECMs 0 and 1, with a tendency to go toward ECM -1 (the MGM), but without reaching the MGM since it is typically kicked back toward ECM 0 or ECM 1, by the antimode -1, which is close to ECM -1. This corresponds to LFF behavior in the laser intensity [Figs. 3(b)χ and 4(c)]. As we further increase κ, the gap between ECM -1 and its antimode widens and the trajectory finally settles on ECM -1, corresponding to CW behavior for the laser [Fig. 4(d)]. With increasing κ, a similar sequence of events occurs again: ECM -1 undergoes bifurcations, a new MGM (ECM -2) appears, dynamics involve several ECMs (LFF), and finally the trajectories settle on the new MGM.

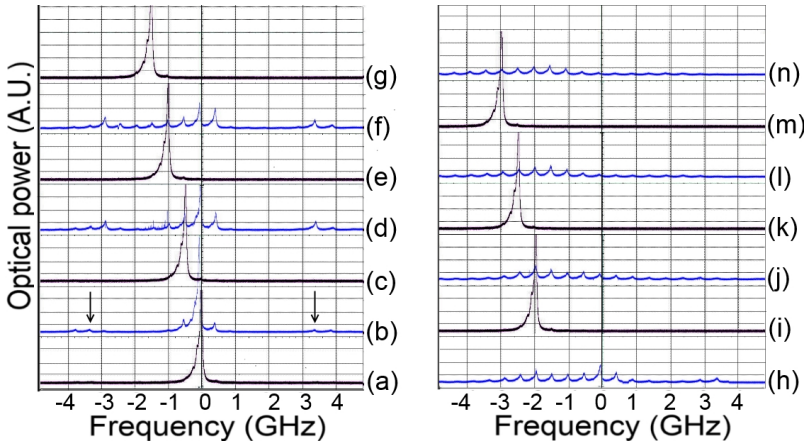

Fig. 5. Experimental optical spectrum with FP interferometer for (a) η= 0.0, (b) 0.10, (c) 0.13, (d) 0.16, (e) 0.18, (f) 0.2, (g) 0.24, (h) 0.26, (i) 0.3, (j) 0.33, (k) 0.35, (l) 0.4, (m) 0.42, and (n) 0.48. I = 11.24 mA and L = 30 cm. The arrows indicate the relaxation sidebands.

#200290 - $15.00 USD Received 7 Nov 2013; revised 20 Jan 2014; accepted 20 Jan 2014; published 28 Jan 2014

To further explore the correspondence between experiment and modeling, we represent the optical spectrum in Fig. 5, for I = 11.24 mA, corresponding to relaxation-oscillation frequency f_{RO} ∼3.2 GHz, as η is increased. It illustrates how the sequence of bifurcations and of ECMs involved corresponds to the numerical predictions. For η ∼0, corresponding to region α of Fig. 2, the optical spectrum of Fig. 5(a) shows that the laser-output power remains in ECM 0, which is close in frequency to the longitudinal mode of the solitary laser (0 GHz). With increasing η, the optical spectrum of Fig 5(b) shows that 2 neighboring ECMs, called ECMs 1 and -1, at ±0.5 GHz, become active, and f_{RO} becomes undamped and is manifested as sidebands, that appear at around ±3.2 GHz from the ECMs [Figs. 2(β) and 5(b)]. For a further increase in η, the spectral peaks at ±0.5 GHz (ECMs 1, -1) become stronger and we observe in the time series of the optical intensity the dropout events typically associated with LFF. As we further increase η, at η = 0.12, instability stops and stable emission occurs on ECM 1, as can be seen in Figs. 2(χ) and 5(c). We then observe that the same sequence of events, *i.e.* the stable ECMs become destabilized and itinerancy between several neighboring ECMs results until the laser stabilizes again on an ECM shifted in frequency by -0.5 GHz. This occurs experimentally for a total of 10 ECMs, over the entire range of experimentally accessible η.

Moreover, in the unstable regions, we systematically identify LFF, and in particular the typical random power dropouts [Fig. 2(β), 2(δ), 2(ϕ), and 2(ι)], until η ∼0.26 is reached. In contrast, for higher η, we do not observe LFF but rather a regime of fully developed coherence-collapse (CC). The two regimes can be easily discriminated experimentally by analyzing the optical spectrum; when the dominant modes are around the LM in unstable regimes [Fig. 5(b), 5(d), 5(f), and 5(h)], LFF is typically observed; in contrast, when the dominant modes are near the MGM [Fig. 5(j), 5(l), and 5(n)], fully developed CC is the observed chaotic behavior. It is important to determine the region of validity of the bifurcation casacade between ECMs as the mechanism leading to fully developed CC. We have observed consistently the presence alternating ”stable” and ”unstable” regions for all values of the current between I_{th} and 1.5 I_{th} . In addition, LFFs are still observed until 1.2 I_{th} when the ECMs lose stability, but the average time between the LFF dropouts typically become shorter, as reported in Ref. [27].

3.1. Varying the current

In order to analyze the effect of I, we compare the experimentally observed bifurcation cascades for I = 11.24 mA [Fig. 2] and 14.69 mA [Fig. 6(a)]. We observe three marked phenomena with increasing I. The first is that alternating stable and unstable regions are still observed, but no longer a systematic cascade involving the successive MGMs. The second is that the cascade exhibits interrupted chaotic behavior above a feedback level that decreases with increasing I. Indeed, we have observed consistently the presence of alternating “stable” and “unstable” regions for all values of the current between I_{th} and 1.5I_{th}. The third is that for larger I, longer (though fewer) regions of stable CW emission exist compared to low I.

Numerical simulations help us interpret the influence of I on the BD. Larger I leads to larger changes in intensity and thus to trajectories that explore a larger region of phase space. Also, at low I, the unstable regions typically correspond to LFF regime, within which a drift toward the MGM is observed. At larger I, the unstable regions typically correspond to fully-developed CC in which chaotic itinerancy between ruins of ECMs is observed, with no drift toward the MGM. This explains why we observe numerically that at larger I, either larger κ is needed to get out of an unstable region and reach the MGM, or the MGM is not reached at all. This in turn explains the “perturbed” bifurcation cascade observed experimentally, in which some of stable regions are skipped because the trajectory never settles on the MGM. Moreover, at large κ, fully developed CC involving ECMs that are far away from the MGM, makes the MGM inaccessible, thus explaining the interrupted bifurcation cascade. Finally, the fact that long stable regions can

#200290 - $15.00 USD Received 7 Nov 2013; revised 20 Jan 2014; accepted 20 Jan 2014; published 28 Jan 2014

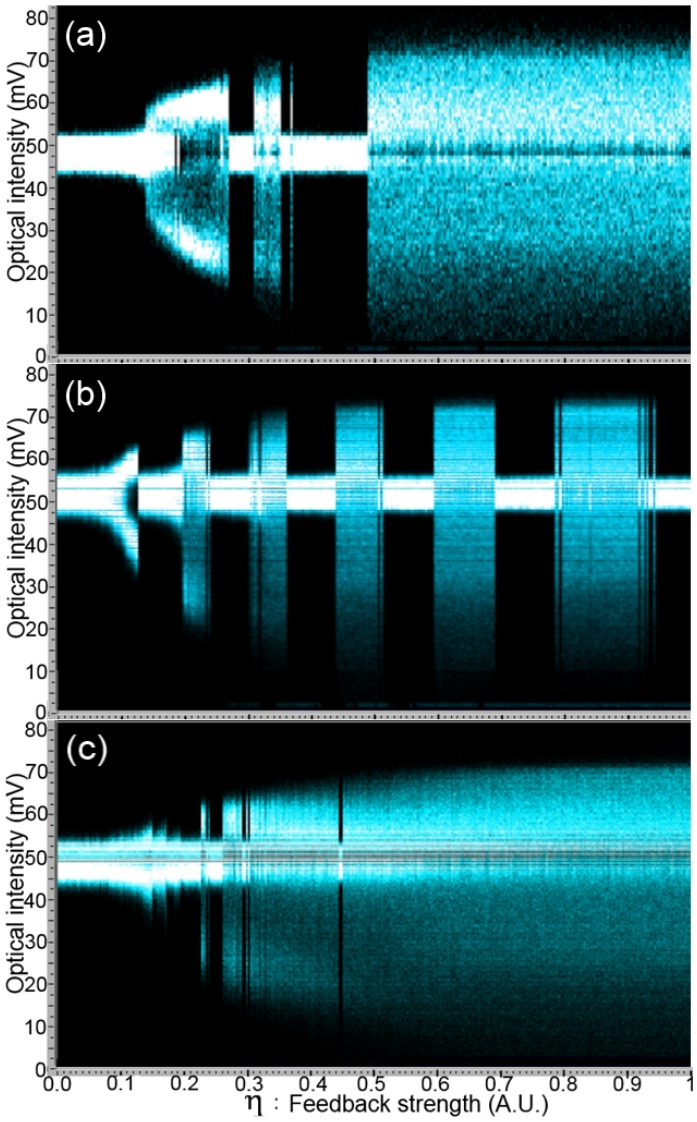

Fig. 6. Experimental BDs for (a) I = 14.69 mA with L = 30 cm, I = 11.24 mA with L = (b) 15 cm and (c) 65 cm.

be observed at larger I stems from the fact that larger κ is needed to destabilize the MGM when I is increased, as shown by the formula 21 in [13]. Thus, when the trajectory reaches the MGM, it needs larger κ to leave it, thus explaining the longer CW regions in the BD.

3.2. Varying the external cavity length

The dependence of the BD on L is explored in Fig. 6(b) and (c). The experiment is executed for L = 15, 30 [Fig. 2], and 65 cm, at I = 11.24 mA. At a short L, we again observe a cascade of bifurcations, but with significantly longer stable regions during which the laser-output power dwells on a single ECM before moving into the subsequent unstable regime, itself followed by the next ECM [Fig. 6(b)]. Moreover, we also observe a well-resolved experimental Hopf

#200290 - $15.00 USD Received 7 Nov 2013; revised 20 Jan 2014; accepted 20 Jan 2014; published 28 Jan 2014

bifurcation of the first ECM that appears in the cascade. In Fig. 6(c), when L = 65 cm, we barely observe a cascade of bifurcations for small η ($0.1 \leq \eta \leq 0.23$). The laser-output power remains briefly on a single ECM, then moves into an unstable regime followed by the next stable ECM over a small range of η and we cannot observe any cascade behavior by further increasing η.

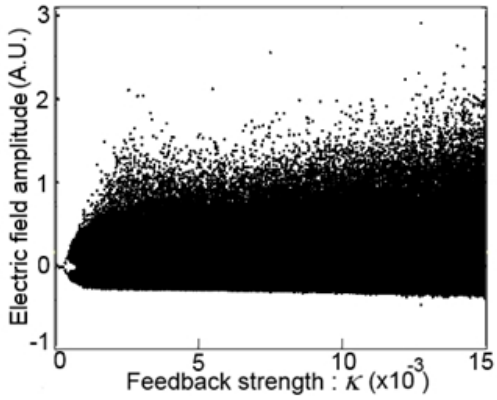

Fig. 7. Numerical BD of p = 1.03, L = 65 cm and $\omega_o \tau = 0$.

Numerical simulations also help us interpret the influence of L on the BD. Figure 7 shows the simulated BD for a long cavity length L = 65 cm. The absence of a cascade is consistent with the experimental results. When L is long, the spectral separation between ECMs is reduced (e.g., 1 GHz→15 cm, 500 MHz→30 cm, 233 MHz→65 cm) in the optical spectrum. Therefore, each participating mode being close in phase space, large-amplitude itinerancy between several modes is easily observed. In the limit of a very long L, Ruiz-Oliveras *et al*. have proven that the laser is always unstable [28]. Indeed, numerical observation of the trajectories on the ellipse shows that the proximity the ECMs impedes the development of independent attractors and thus prevents the existence of a BD. Conversely, increased distance between the ECMs for shorter L means that larger η is needed before attractor merging occurs, thus explaining the longer stable regions.

4. Discussion

We compared both forward (increasing η) and reverse (decreasing η) BDs. Although we can observe the cascade behavior in both cases, the transitions between stable and unstable regions occur for smaller feedback levels in the reverse cascade. This difference results from the fact that as the feedback is decreased, the trajectory in an unstable regime does not switch toward a neighboring CW ECM as soon as this ECM becomes stable but tends to remain in its current unstable regime. On the contrary, when the feedback is increased and the laser is in a stable regime, the trajectory, by definition, leaves the stable attractor as soon as it becomes unstable. The inclusion of noise in the LK model, through the addition of langevin noise sources, blurs the simulated BDs, makes them closer-looking to the experimental ones, and does not alter the main features of the cascades. This observation confirms the deterministic origin of bifurcation cascades in ECSLs.

Under highly stabilized temperature and I and good resolution of feedback strength i.e. controlling the angle of QWP, it is interesting to point out that Fig. 6(b) shows, for the first time to our knowledge, a well-resolved experimental Hopf bifurcation in an ECSL ($\eta \sim 0.1$). It corresponds to the loss of stability by the ECM that is first created (ECM 0) when η is increased,

#200290 - $15.00 USD Received 7 Nov 2013; revised 20 Jan 2014; accepted 20 Jan 2014; published 28 Jan 2014

and to the birth of a stable limit cycle. The conditions of this observation can be interpreted in light of the trajectory in phase space. In Fig. 4, it is clear that since ECM 0 does not have a partner antimode, it has more room to develop in phase space than any other ECM so that it is more likely to dominate over. This potential is fully unleashed in the case of small cavities since ECMs 1 and -1 are distant in phase space from ECM 0 and allow for large-amplitude instabilities to develop locally around ECM 0, before attractor merging occurs.

5. Conclusion

In this paper, we have presented a global picture of the dynamics of an external-cavity DFB laser diode, in the long-cavity case, and when subjected to low-to-moderate current injection, by means of experimental BDs and optical spectrum analysis. We determine the region of validity of the bifurcation cascade between ECMs as the mechanism leading to fully developed CC. We observe consistently the presence alternating "stable" and "unstable" regions for all values of the current between I_{th} and 1.5 I_{th}. Moreover, in the unstable regions, we systematically identify LFF, and in particular its typical random power dropouts with lower η. In contrast, for higher η, we do not observe LFF but a regime of fully developed CC. Also, we further experimentally study the evolution of the bifurcation cascade when L or I is varied. We verify that the cascade gradually disappears, as L or I is increased, because of attractor merging. We have further explained the qualitative features of the observed BDs in light of the LK model.

Acknowledgments

The authors acknowledge the support of the Conseil Regional of Lorraine, GT-CNRS2958, and National Science Foundation by ECCS Grants No. 0925713.

#200290 - $15.00 USD Received 7 Nov 2013; revised 20 Jan 2014; accepted 20 Jan 2014; published 28 Jan 2014